

ATOMISTIC- AND MESO-SCALE COMPUTATIONAL SIMULATIONS FOR DEVELOPING MULTI-TIMESCALE THEORY FOR RADIATION DEGRADATION IN ELECTRONIC AND OPTOELECTRONIC DEVICES

Fei Gao

**University of Michigan
2355 Bonisteel Blvd.
Ann Arbor, Michigan 48109-2014**

13 Feb 2017

Final Report

APPROVED FOR PUBLIC RELEASE; DISTRIBUTION IS UNLIMITED.



**AIR FORCE RESEARCH LABORATORY
Space Vehicles Directorate
3550 Aberdeen Ave SE
AIR FORCE MATERIEL COMMAND
KIRTLAND AIR FORCE BASE, NM 87117-5776**

DTIC COPY

NOTICE AND SIGNATURE PAGE

Using Government drawings, specifications, or other data included in this document for any purpose other than Government procurement does not in any way obligate the U.S. Government. The fact that the Government formulated or supplied the drawings, specifications, or other data does not license the holder or any other person or corporation; or convey any rights or permission to manufacture, use, or sell any patented invention that may relate to them.

This report is the result of contracted fundamental research deemed exempt from public affairs security and policy review in accordance with SAF/AQR memorandum dated 10 Dec 08 and AFRL/CA policy clarification memorandum dated 16 Jan 09. This report is available to the general public, including foreign nationals. Copies may be obtained from the Defense Technical Information Center (DTIC) (<http://www.dtic.mil>).

AFRL-RV-PS-TR-2016-0161 HAS BEEN REVIEWED AND IS APPROVED FOR PUBLICATION IN ACCORDANCE WITH ASSIGNED DISTRIBUTION STATEMENT.

//SIGNED//
DAVID CARDIMONA
Program Manager

//SIGNED//
DAVID CARDIMONA
Technical Advisor, Space Based Advanced Sensing
and Protection

//SIGNED//
JOHN BEAUCHEMIN
Chief Engineer, Spacecraft Technology Division
Space Vehicles Directorate

This report is published in the interest of scientific and technical information exchange, and its publication does not constitute the Government's approval or disapproval of its ideas or findings.

Approved for public release; distribution is unlimited.

REPORT DOCUMENTATION PAGE				Form Approved OMB No. 0704-0188	
Public reporting burden for this collection of information is estimated to average 1 hour per response, including the time for reviewing instructions, searching existing data sources, gathering and maintaining the data needed, and completing and reviewing this collection of information. Send comments regarding this burden estimate or any other aspect of this collection of information, including suggestions for reducing this burden to Department of Defense, Washington Headquarters Services, Directorate for Information Operations and Reports (0704-0188), 1215 Jefferson Davis Highway, Suite 1204, Arlington, VA 22202-4302. Respondents should be aware that notwithstanding any other provision of law, no person shall be subject to any penalty for failing to comply with a collection of information if it does not display a currently valid OMB control number. PLEASE DO NOT RETURN YOUR FORM TO THE ABOVE ADDRESS.					
1. REPORT DATE (DD-MM-YY) 13-02-2017		2. REPORT TYPE Final Report		3. DATES COVERED (From - To) 18 Aug 2015 – 7 Dec 2016	
4. TITLE AND SUBTITLE Atomistic- and Meso-Scale Computational Simulations for Developing Multi-Timescale Theory for Radiation Degradation in Electronic and Optoelectronic Devices				5a. CONTRACT NUMBER FA9453-15-1-0084	
				5b. GRANT NUMBER	
				5c. PROGRAM ELEMENT NUMBER 62601F	
6. AUTHOR(S) Fei Gao				5d. PROJECT NUMBER 4846	
				5e. TASK NUMBER PPM00015486	
				5f. WORK UNIT NUMBER EF126376	
7. PERFORMING ORGANIZATION NAME(S) AND ADDRESS(ES) University of Michigan 2355 Bonisteel Blvd. Ann Arbor, Michigan 48109-2014				8. PERFORMING ORGANIZATION REPORT NUMBER	
9. SPONSORING / MONITORING AGENCY NAME(S) AND ADDRESS(ES) Air Force Research Laboratory Space Vehicles Directorate 3550 Aberdeen Ave., SE Kirtland AFB, NM 87117-5776				10. SPONSOR/MONITOR'S ACRONYM(S) AFRL/RVSW	
				11. SPONSOR/MONITOR'S REPORT NUMBER(S) AFRL-RV-PS-TR-2016-0161	
12. DISTRIBUTION / AVAILABILITY STATEMENT Approved for public release; distribution is unlimited.					
13. SUPPLEMENTARY NOTES					
14. ABSTRACT This project will support a research effort at the University of Michigan to simulate atomistic- and meso-scale behavior of defect evolutions in compound semiconductors, including ultrafast displacement cascade, intermediate defect stabilization and cluster formation, as well as slow defect reaction and migration. The fundamental mechanisms and knowledge gained from atomic- and meso-scale simulations will be input into rate-diffusion theory as initial conditions to calculate the steady-state distribution of point defects in a mesoscopic layered-structured system, thus allowing the development of a multi-timescale theory to study radiation degradation in electronic and optoelectronic devices.					
15. SUBJECT TERMS barrier, detector, infrared, unipolar					
16. SECURITY CLASSIFICATION OF:			17. LIMITATION OF ABSTRACT Unlimited	18. NUMBER OF PAGES 30	19a. NAME OF RESPONSIBLE PERSON David Cardimona
a. REPORT Unclassified	b. ABSTRACT Unclassified	c. THIS PAGE Unclassified			19b. TELEPHONE NUMBER (include area code)

(This page intentionally left blank)

Table of Contents

1. SUMMARY -----	1
2. INTRODUCTION -----	1
3. METHODS, ASSUMPTIONS, AND PROCEDURES -----	2
3.1. Molecular Dynamics Model of Displacement Energy -----	2
3.2. Molecular Dynamics Model of Defect Generation -----	4
3.3. Interatomic Potentials -----	4
3.4. NIEL Model -----	5
4. RESULTS AND DISCUSSIONS -----	6
4.1. Displacement Energies -----	6
4.1.1. Unit Stereographic Triangles -----	7
4.1.2. Threshold Displacement Energy Contour Maps -----	7
4.1.3. Overview of E_d -----	9
4.2. Displacement Cascades and Effective NIEL -----	9
4.2.1. Defect Generation -----	9
4.2.2. Effective NIEL -----	14
5. CONCLUSIONS -----	16
REFERENCES -----	18
LIST OF ACRONYMS -----	21

LIST OF FIGURES

Figure	Page
1. (a) GaAs crystal structure; (b) illustration of stereographic triangles on a reference sphere.....	3
2. (a) The displacement threshold energy around the sides of the unit stereographic triangles for Ga; (b) the displacement threshold energy around the side of the unit stereographic triangles for As.....	7
3. (a) Threshold energy map for Ga; (b) threshold energy map for As.....	8
4. Atomistic configurations of a typical 10 keV cascade in GaAs at (a) the peak damage and (b) the final damage state, where only defects are shown. The defects are identified by size and color, as indicated by different spheres.....	10
5. The number of displaced atoms, including Ga and As displacements and antisites, as a function of time for the 10 keV cascade shown in Fig. 4.....	11
6. The final defect states of (a) 2 keV, (b) 5 keV and (c) 20 keV cascade in GaAs from which can be clearly seen the transition from a single pocket of atomic displacements to multiple subcascades.....	12
7. The number of surviving defects produced in the cascades as a function of PKA energy, where Ga and As interstitials, as well as antisite defects, are presented separately.....	13
8. The total defects of the final damages as a function of the energy density deposited by a PKA, where the solid line represents the fits to MD data.....	14
9. The NIEL obtained based on the MD results for several different incident particles in GaAs, where the values of the NIEL calculated by an analytical approach are imposed for comparison.....	16

ACKNOWLEDGMENTS

This material is based on research sponsored by Air Force Research Laboratory under agreement number FA9453-15-1-0084. The U.S. Government is authorized to reproduce and distribute reprints for Governmental purposes notwithstanding any copyright notation thereon.

DISCLAIMER

The views and conclusions contained herein are those of the authors and should not be interpreted as necessarily representing the official policies or endorsements, either expressed or implied, of Air Force Research Laboratory or the U.S. Government.

(This page intentionally left blank)

1. SUMMARY

This project will support a research effort at the University of Michigan to simulate atomistic- and meso-scale behavior of defect evolutions in compound semiconductors, including ultrafast displacement cascade, intermediate defect stabilization and cluster formation, as well as slow defect reaction and migration. The fundamental mechanisms and knowledge gained from atomic- and meso-scale simulations will be input into rate-diffusion theory as initial conditions to calculate the steady-state distribution of point defects in a mesoscopic layered-structured system, thus allowing the development of a multi-timescale theory to study radiation degradation in electronic and optoelectronic devices. The long-term goal is developing a fundamental understanding of defects and defect processes in compound semiconductors, including defect/property relationships, the effects of defects on transport processes, the aggregation of defects to form complex nanostructures, and the development of predictive models of behavior.

2. INTRODUCTION

It is well known that in a perfect crystal, the continuous free-electron states are quantized into many Bloch bands separated by energy gaps. These Bloch electrons move freely inside the crystal with an effective mass different from the free-electron mass [1]. In the presence of defects, however, the field-driven current flow of Bloch electrons in the perfect crystal will be scattered locally by these defects, leading to a reduced electron mobility. Also, the photo-excited electron lifetime, due to non-radiative recombination with defects, has been proven to be a key factor affecting the sensitivity or the performance of optoelectronic devices (e.g., photo-detectors and light-emitting diodes) [2]. The dangling bonds attached to the point defects may capture extra electrons to form charged defects. In this case, the positively-charged holes in the system will be trapped to produce a strong space-charge field, while the negatively-charged electrons may generate the so-called $1/f$ -current noise in their bumpy motions due to the presence of many potential minima and maxima from randomly-distributed charged defects. Therefore, understanding of defect production, stabilization, clustering, migration and interaction with microstructural features is crucial for developing a multi-scale theory to explore radiation degradation in electronic and optoelectronic devices. At the most fundamental level, molecular dynamics can be used to study defect production, migration and interaction, while kinetic Monte Carlo methods can be employed to simulate defect evolution and their spatial distribution. The researchers at University of Michigan have extensive experience performing atomic- and meso-scale simulations of defect production and evolution in semiconductors.

The current project focuses on one particular semiconductor, namely gallium arsenide (GaAs), because it has received considerable attention due to its potential electronic applications, such as GaAs-based metal semiconductor field effect transistors and logic gates, near-infrared imaging devices and photovoltaic nodules [3]. As a means for fabricating compound semiconductors, the interest in using ion implantation continuously increases, which inevitably introduces defects. The diffusion and accumulation of these defects are critical factors controlling the dynamics of ion implantation processes and device degradation, as well as affecting charge compensation, minority-carrier lifetimes and luminescence efficiencies. Recently, use of GaAs in high-power space-energy systems and special space-probe applications has been proposed. However, space radiation damage to the GaAs may be a limiting factor on interplanetary missions

unless sufficient shielding is provided to keep damage levels under acceptable limits. Consequently, radiation damage studies have been made experimentally on the effects of electron [4], and proton and neutron irradiation [5], including defect production and annealing, as well as effects on the performance of GaAs devices. On the other hand, understanding the basics of ion-solid interaction and irradiation damage has led to significant developments in state-of-the-art atomic-level, kinetic Monte Carlo and meso-scale simulations, and these simulations have dramatically advanced the knowledge of defects and defect processes in a number of materials, ranging from metals [6,7] to semiconductors [8] to ceramics [9,10]. Recently, large-scale *ab initio* and classical molecular dynamics (MD) methods have been developed for the study of radiation damage in semiconductors [11,12], and these methods are used to explore the number of displacements produced, defect clustering and disordering, as well as the effects of charge transfer and charge-density redistribution on the dynamics and ultimate charge-state of defect formation. These simulations have demonstrated some nonlinear effects taking place at low and high energies, which can greatly modify the number of displacements as predicted by the simplified Kinchin-Pease model.

It has been long realized that the observed radiation damage to electronic components made from semiconductors or semiconducting compounds is proportional to the non-ionizing energy loss (NIEL) [13]. Consequently, the experimental use of NIEL for correlating proton-induced displacement damage in semiconductor devices has been widely applied over the past decade, which has proven useful in the study of both Si and GaAs [14,15]. Moreover, radiation damage in other semiconductors such as diamond and SiC [16], and many III-V compounds, such as InP [17], has been investigated using the NIEL concept. Previously, several models have been developed to estimate the NIEL in GaAs using a Monte Carlo charged particle transport code [18] or based on an empirically determined damage efficiency [19]. Although these models provide significant insights into the correlation between the NIEL and displacement damage, there remain discrepancies between proton NIEL calculations and experimental measurements in GaAs devices. Determining accurate damage levels and improving the NIEL model have been an ongoing focus of the Space Radiation Effects Community (SREC). In light of this, we have employed a molecular dynamics method to simulate defect production, defect clustering and disordering, as well as initial kinetic energy density in GaAs. In these simulations, the damage state following each cascade was characterized and analyzed for defect distribution and amorphization. Based on MD results, we have developed a new energy partition function model, which was then used to determine the NIEL in GaAs. The present approach provides a general method for accurately calculating the NIEL for fast neutrons, protons and heavier particles.

3. METHODS, ASSUMPTIONS, AND PROCEDURES

3.1. Molecular Dynamics Model of Displacement Energy

A modified version of the Molecular Dynamics (MD) code-MOLDY [20] was employed to determine the threshold displacement energies along different recoil directions. A simulation box with a size of 10x10x10 unit cells (consisting of 8,000 atoms) was created, with a zinc-blende structure for GaAs, as shown in Fig.1(a). Periodic boundary conditions were applied to the system. During the simulation, the computational block was held at a temperature at 0 K, and equilibrated for 5 ps prior to a recoil event. To simulate a recoil event, a recoiling atom was created by defining

either Ga or As as a primary knock-on atom (PKA), which was chosen close to the center of simulation block to prevent the PKA from crossing the boundaries. Furthermore, the PKA was given a kinetic energy (starting at 6 eV) along a specific crystallographic direction and the dynamic process was evolved for 5000 MD time steps (about 5ps in real time). If the amount of energy given was enough to overcome the threshold displacement energy, the PKA was initiated by displacing it from its original site to generate a stable Frenkel pair or anion anti-site at the end of the simulation. On the other hand, if a stable defect configuration was not observed, the initial kinetic energy was increased by 2 eV, and so E_d , quoted here is ± 1 eV.

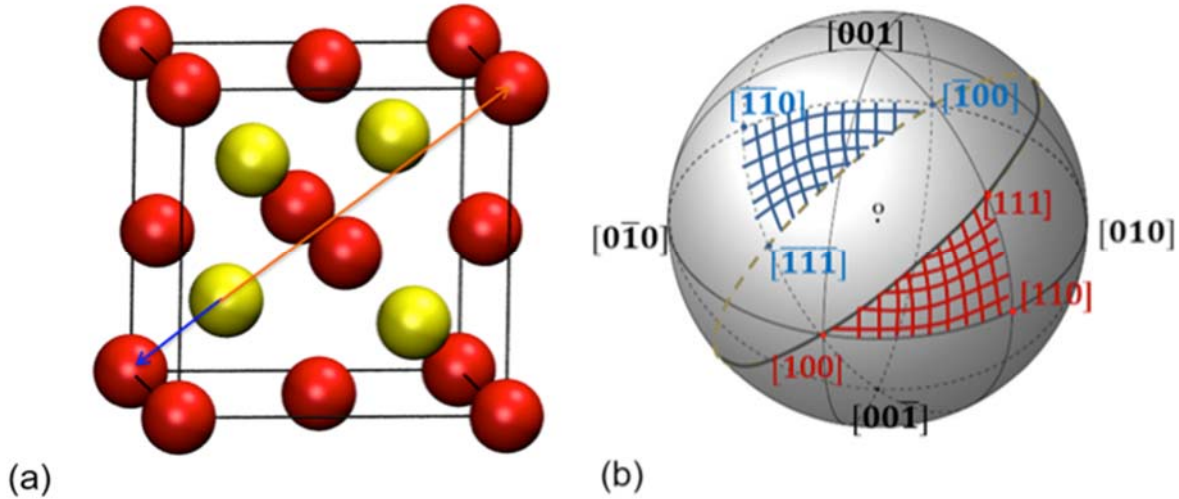


Fig. 1 (a) GaAs crystal structure; (b) illustration of stereographic triangles on a reference sphere.

Consideration of crystallographic geometry has been proven to be a distinctive factor in exploring the displacement damage [21]. In this study, we use the Mercator method [22] to represent the stereographic projection of the crystallographic direction of the zinc-blende crystal, which can be thought to be equivalent to the diamond structure. Each point on the reference sphere in Fig. 1(b) stands for a direction projection, where the sphere center coincides with the origin of the crystal cube. For zinc-blende, a standard unit stereographic triangle on the sphere is representative of the area in which all possible recoil directions can take place, with the remaining directions known to exhibit the same behavior [22]. However, for a compound semiconductor, e.g. GaAs, which has the nearest neighbor of unlike atoms, two triangles are required (with the side of $[100]$ - $[110]$ - $[111]$ and $[\bar{1}00]$ - $[\bar{1}\bar{1}0]$ - $[\bar{1}\bar{1}\bar{1}]$, respectively) to investigate the displacement threshold energy for each atom type. For example, an As atom moving along the $[111]$ direction, as indicated by an orange arrow in Fig. 1(a), encounters a Ga atom at the distance of 7.34 Å, but at a distance of 2.45 Å when it moves along the $[\bar{1}\bar{1}\bar{1}]$ direction. This should make the displacement of As atoms difficult along $[111]$ and much easier along $[\bar{1}\bar{1}\bar{1}]$. This fact has been illustrated in Fig. 1(b), with red shaded part corresponding to the triangle in positive direction while the blue one is for negative. Thus, more than 3600 directions in total were simulated for both species as a PKA indicated by the angles in Mercator map.

3.2. Molecular Dynamics Model of Defect Generation

To simulate displacement cascades, periodic boundary conditions were also applied in three directions, and the lattice temperature was initially selected to be 100 K, which mimics a thermal energy just about the zero-point value. All the simulations are carried out with constant volume and constant number of atoms. The MD-cell size is selected to avoid overlap of a displacement cascade with itself due to the periodicity. For a displacement cascade of 20 keV, a crystal of 1,000,000 atoms (50x50x50 unit cells) is employed for simulation. Before the primary recoil is initiated, the perfect crystal block is allowed to equilibrate for 10 ps at 100 K to achieve an equilibrium phonon state. The cascades are initiated by giving a primary knock-on atom (PKA) a kinetic energy along a randomly-selected direction. In the present study, only Ga PKA events are simulated, but the simulations can be extended to As PKAs. Furthermore, the collision cascade produces secondary As knock-on atoms, which contribute to the overall damage production. The evolution of each cascade is examined for about 20 ps following the primary knock-on event, after which the number of defects shows no significant change. We have simulated the displacement cascades in the energy range from 500 eV to 20 keV, and 20 PKA events are carried out at each energy to obtain meaningful statistics. A Wigner-Seitz cell method is employed to identify vacancies, interstitials and antisite defects. A lattice site with no atoms is designated as a vacancy, the cell with two atoms where one is recognized as an interstitial with the site occupied by the wrong atom type is defined as an antisite defect.

3.3. Interatomic Potentials

The interactions between Ga-Ga, Ga-As and As-As are described using analytical bond-order potentials (BOPs) developed by Albe et al. [23]. The potentials have been used to study a wide range of properties of GaAs compound structures, as well as the pure phases of gallium and arsenic, including non-equilibrium configurations. The numerical results on point defect properties, surface properties, and melting behavior have been used to validate the accuracy and transferability of the potentials [23]. Point-defect properties and surfaces with low As content are found to be in good agreement with literature results, and the molten GaAs is found to be consistent with a structural model based on experiments that indicate a polymerized arsenic phase in the melt. However, in order to simulate the interaction of high energy particles with GaAs, the short-range interactions have been further modified to match the ‘Universal’ screening function Ziegler-Biersack-Littmark (ZBL) potential [24] that gives a good representation of high energy scattering of atoms in solids. This is achieved by coupling the original BOPs and the short-range function through the use of the Fermi function

$$F(r) = \frac{1}{1 + e^{-b_f(r-r_f)}}, \quad (1)$$

where $F(r)$ quickly goes to one as r increases. The total potential is given by connecting the BOP to the ZBL potential:

$$V(r) = V_{ZBL} [1 - F(r)] + V_{BOP} F(r), \quad (2)$$

which yields a repulsive potential that is dominated by the ZBL for very short distance and quickly approaches the BOP as r increases, as desired. The parameters of b_f and r_f are adjusted to make sure that the potential and its first derivative are smoothly transitioned. The values of b_f are determined to be 14, 14 and 7.5 \AA^{-1} , and those of r_f are 0.95, 0.95 and 0.65 \AA for Ga-Ga, Ga-As and As-As interactions, respectively. We have employed these potentials to study the threshold energies of Ga and As [25], and the results are in good agreement with those obtained by both first principles calculations and experimental methods. The formation energies of vacancies are determined to be 2.0 and 2.4 eV for the As and Ga sublattices, respectively. Several configurations of self-interstitial atoms (SIA) are found to be stable in the static lattice, and the most stable interstitial is an As-As<100> dumbbell centered on As sites with the formation energy of 5.88 eV. The results are in reasonable agreement with those found in *ab initio* calculations. Nevertheless, these results suggest that the model potentials are well suited for studying displacement cascades in GaAs.

3.4. NIEL Model

Several models have been previously developed to determine the NIEL in Si [26] and GaAs [27]. Conventionally, the NIEL can be determined through the so called Lindhard energy partition function, $G(T)$ [28]

$$NIEL = \alpha \int_{E_d}^{T_{max}} T \frac{d\sigma}{dT} G(T) dT, \quad (3)$$

where α is the atomic density of the target material, T the kinetic energy of the recoil, T_{max} the maximum energy that can be transferred to a recoil nucleus by an incident particle and E_d the threshold displacement energy which is conventionally taken to be 25 eV. $G(T)$ is the energy partition function and $d\sigma/dT$ the differential interaction cross section. At low energy, the recoil energy of a PKA, E_{PKA} , is close to T , but at high energy most of the energy of a PKA contributes to ionization. Also, the number of displacements can be estimated through $G(T)$ by the Kinchin-Pease model. Based on this model, the NIEL can be rewritten as

$$NIEL = \alpha \int_{E_d}^{T_{max}} F(T) G(T) \frac{d\sigma}{dT} dT, \quad (4)$$

where $F(T) = E_d N_F / 0.4$. It is well known that the number of defects produced by a PKA, N_F , is linearly proportional to the recoil energy in the Kinchin-Pease model, which means that in this model the NIEL becomes proportional to the number of defects produced by irradiation. However, it has been recognized that the NIEL is not necessarily proportional to the number of defects, due to non-linear processes that take place in semiconductors, particularly associated with the formation of multiple disordered regions or amorphous pockets. In the present study, we have used a MD method to simulate defect production where non-linear processes will be simultaneously taken into account. Based on our MD results, we introduce an “effective NIEL” that depends on the number of defects in the material, i.e.,

$$NIEL = \alpha \int_{E_d}^{T_{max}} \frac{E_d}{0.4} N_F^{MD} G(T) \frac{d\sigma}{dT} dT \quad (5)$$

$N_F^{MD}(T)$ is the number of defects produced at a given recoil energy of T , as obtained by MD simulations.

Many different forms of screened Coulomb potentials are proposed to calculate the differential interaction cross section, including Bohr, Thomas-Fermi, Lindhard, Molere and ZBL potentials [29]. Considering that the ZBL Universal Formalism is based on experimentally determined interatomic potentials, this formalism is generally used to calculate the differential interaction cross section, as given by

$$\frac{d\sigma}{dt} = \frac{-\pi a_U^2}{2} \frac{f(t^{1/2})}{t^{3/2}} \quad (6)$$

where $t = \varepsilon^2 T / T_{max}$ is a dimensionless collision parameter related to recoil energy T , ε is the ZBL reduced energy and a_U is the ZBL Universal screening length. The function of $f(t^{1/2})$ is referred to as the Thomas-Fermi scattering function, as detailed in references [26,29]. A simplified version of the Lindhard energy partition function is used for the present study [26]:

$$G(T) = \frac{1}{1 + k_d g(\varepsilon_d)} \quad (7)$$

where k_d , ε_d and $g(\varepsilon_d)$ are dimensionless parameters, and their detailed formulas and values are described elsewhere [26].

4. RESULTS AND DISCUSSIONS

4.1. Displacement Energies

Within the GaAs microstructure, a distinct threshold energy exists for each crystallographic direction. In the following sections, the threshold displacement energies on both sides and for the inner part of unit stereographic triangles will be established. For a detailed description of defect configurations and separation distance, we will present these at the end of the recoil events, which can be used to explain the corresponding values of E_d in low index directions.

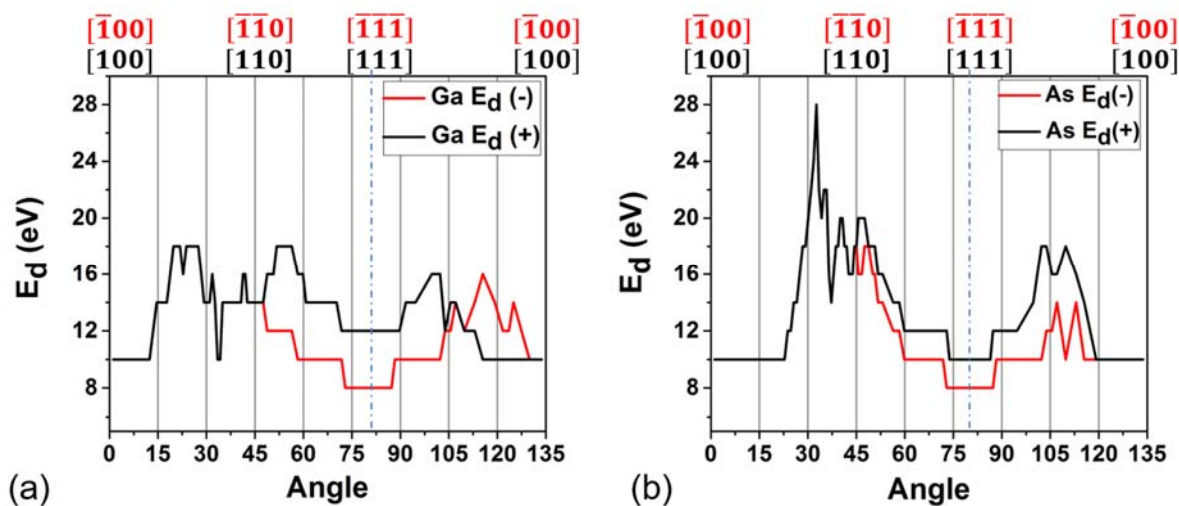


Fig. 2 (a) The displacement threshold energy around the sides of the unit stereographic triangles for Ga; (b) the displacement threshold energy around the sides of the unit stereographic triangles for As.

4.1.1. Unit Stereographic Triangles

The calculated threshold energies for Ga and As recoil atoms on the three borders of the two unit stereographic triangles are illustrated in Fig. 2(a) and Fig. 2(b), respectively. It was noticed that both Ga and As atoms require at least 8 eV kinetic energy to knock off a neighbor atom along a given direction. This is the lowest energy value for which a stable Frenkel pair was created through the simulations. For both triangles considered, the threshold energy of a Ga PKA varies over a range of 8 eV to 18 eV along the sides of the triangles, as shown in Fig. 2(a), while As was widely distributed between 8 eV and 28 eV in Fig. 2(b). A lower value of energy of 8 eV in the $[\bar{1}\bar{1}\bar{1}]$ direction than that of 12 eV in the $[111]$ direction was noticed for Ga. The higher value in $[111]$ for Ga can be explained by the strong repulsive energy between Ga and its first nearest neighbor As, thus forcing it to return to its equilibrium site during collision. However, for the As case (Fig. 2b), the displacement threshold energy for these two directions was 8 eV and 10 eV, respectively. This could be explained by the energy transfer efficiency of the heavy PKA to a lighter atom, thus the difference in the two directions for an As atom was not significant, though a larger distance to Ga in $[111]$ direction would make for a slight difference in the value. Furthermore, a Ga atom is 1.13 lighter than an As atom, and thus it should be easier for an As to knock off a Ga from its lattice position than vice versa. However, in monatomic diamond structured semiconductors (e.g. Si), it has been shown that E_d is equivalent in all $\langle 111 \rangle$ directions [30]. The differences noticed here will be further discussed in Section 4.2.

4.1.2. Threshold Displacement Energy Contour Maps

In addition to the E_d determined along the main crystallographic directions, a large number of directions within the stereographic projection triangles were also taken into consideration as a

function of angles. The results are interpreted by Mercator maps. As mentioned before, over three thousand recoil events were performed for both Ga and As to get a smooth and comprehensive distribution, and an in-depth understanding of E_d dependence on crystallographic orientation, and the results are shown in Figs. 3(a) and (b) for Ga and As recoils, respectively, where the different colors indicate different energy scales. Thus, we can consider the E_d as defining three distinctive regimes, namely zone 1, 2 and 3 as indicated in the figures. An interesting observation is that there is an even higher value of threshold energy of 22 eV for Ga, which occurs to trigger the recoil events in the central part of the stereographic projection triangles, while a maximum of 18 eV is found along the directions on the sides for Ga, as described in Section 3.1. This may be due to the collision of the PKA with the secondary nearest neighbor atoms after moving a longer distance. Comparing the two triangles depicting the displacement energies of Ga recoils (Fig. 3a), there is a clear quantitative difference between the negative and positive directions. This is especially true in the inner region (zone 2) where the fraction of Ga recoils that produce persistent defects appears to be higher in the positive direction, with an initial energy of 18 eV, consistent with the larger distribution of 18 eV on the positive side than that on the negative side. Threshold energies for Ga PKAs in the $[111]$ direction and 20 degrees north of the (110) pole, denoted as zone 1, are 4 eV greater than those along the $[\bar{1}\bar{1}\bar{1}]$ direction. Further, the region enclosed by zone 2 reaches a maximum threshold of 22 eV, while the corresponding region on the negative side comes with a maximum of 18 eV.

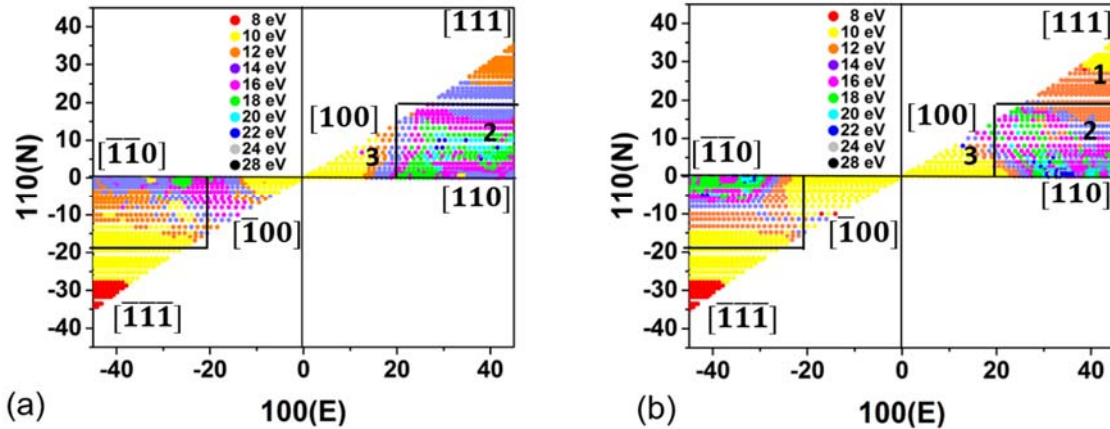


Fig. 3 (a) Threshold energy map for Ga; (b) threshold energy map for As.

Similarly, for As PKAs (Fig. 3b), a maximum value of 28 eV (E_d) has been found in zone 2 which can also be interpreted by the same mechanism of collision with a secondary nearest neighbor as Ga. Overall, while there are small differences in the region adjacent to the $[100]$ direction (zone 3), large differences are noticed in zone 1 and zone 2. This indicates that there is a higher probability of producing a stable defect with small energies in zone 3, than in either zone 1 or zone 2.

Table 1. Overview of displacement energies compared with experiment data.
($E_{d,ave}$, average displacement energy over three thousand directions for each type; $N_{direction}$, number of directions simulated for each type.)

Recoil type	$N_{direction}$	$E_{d,ave}$ (eV)	E_d (eV)						Experiment
			[100]	$[\bar{1}11]$	[110]	$[\bar{1}\bar{1}0]$	[111]	$[\bar{1}\bar{1}\bar{1}]$	
Ga	1828	13.38	10	10	14	14	12	8	10.0±0.7 [32]
As	1828	12.75	10	10	18	18	10	8	9 [32]

4.1.3. Overview of E_d

The average displacement threshold energies in two oppositely oriented stereographic triangles for each atom type are summarized in Table 1. The average threshold energies over the statistically significant sample size (few thousand directions) combining both positive and negative directions were found to be 12.75 and 13.38 eV for As and Ga, respectively. The almost identical value of $E_{d,ave}$ (small difference of 0.63 eV) is to be expected due to the many physical similarities between these two atoms. Moreover, there have also been several experimental studies in GaAs on examining primary damage response. The lowest energy threshold from the experimental estimation of 10.0±0.7 eV and 9 eV [31] is consistent with 8 eV at the minimum for both species from our simulations. This indicates a good match with the established data in crystallographic non-equivalent crystal directions. In addition, since the effective displacement energy is typically about 50% higher than the threshold [32] an estimation value of 15 eV on top of experiment data is consistent with what we have obtained through MD simulations (13.1±0.3eV). Hence, they are in satisfactory agreement.

4.2. Displacement Cascades and Effective NIEL

4.2.1. Defect Generation

Similar to other semiconductors, the displacement cascades modeled in the present work exhibit two basic phases, i.e. a ballistic phase and a recombination phase. Here, the former lasts a few tenths of ps, during which the primary recoil atom initiates an avalanche of atomic displacements, resulting in many atoms being displaced. After the number of displacements reaches a maximum, the system starts to cool down and the follow-up recombination occurs, causing some of these displacements to recombine with the empty lattice sites. At about 5 ps, the

cascade process reaches a stable state with occasional interstitial rotation, but without significant defect migration. The peak and final damage states of a typical 10 keV cascade in GaAs are shown in Figs. 4(a) and (b), respectively, where only displaced atoms are plotted. The interstitials are represented by large spheres and vacancies by small ones, as indicated in the legend. The Ga PKA in this simulation traveled about 10 nm before it came to rest in the lattice, generating multiple damage domains along its path. These domains form distinct regions separated from each other, within which a large number of atoms are displaced. The final damage is very similar to the peak damage in the case of GaAs, but with slightly smaller number of displacements. It is surprising that the recombination of displaced atoms with the empty lattice sites is small, in contrast to the displacement cascades in SiC [33] and metals [34] where 50% and 90% of the displaced atoms recombine with vacancies, respectively. This may be associated with the low threshold energies of GaAs [25] where a PKA is able to create large disordered regions along its path, leading to the formation of amorphous domains, which prevents defect recombination at low temperatures. Fig. 4(b) clearly shows that the damage consists of multiple disordered regions or defect clusters, in contrast to SiC where most defects are single interstitials and mono-vacancies, and only a small proportion of the interstitials are found in clusters.

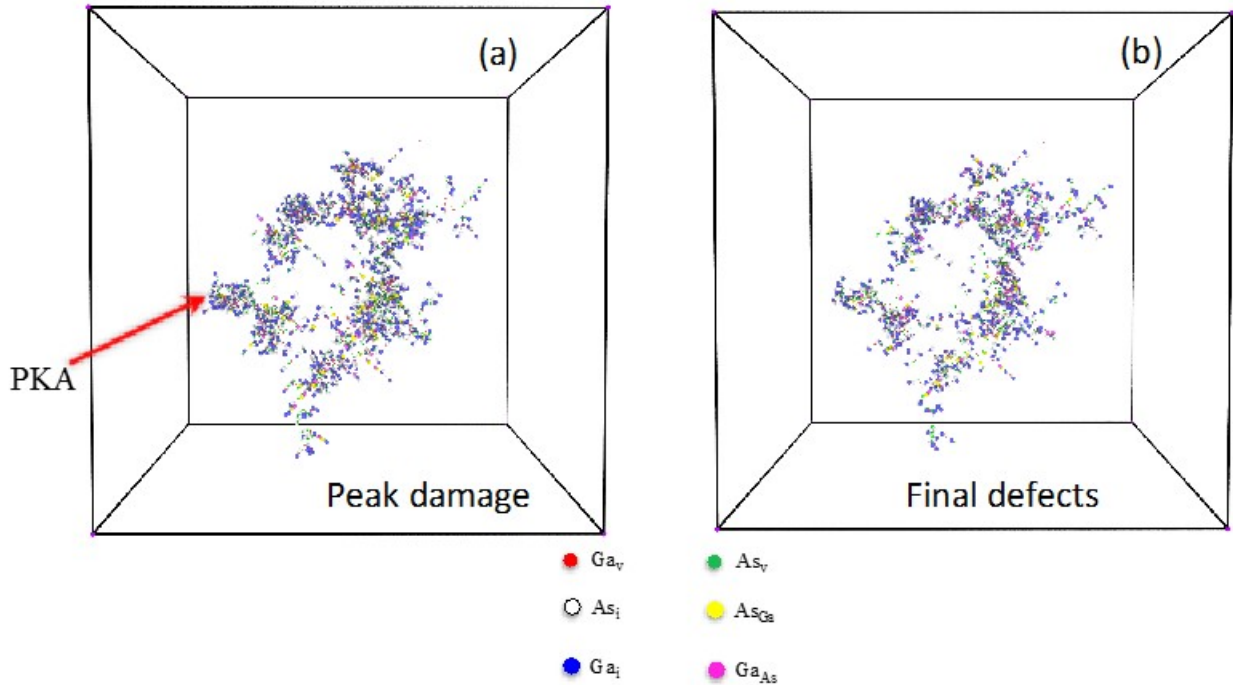


Fig. 4 Atomistic configurations of a typical 10 keV cascade in GaAs at (a) the peak damage and (b) the final damage state, where only defects are shown. The defects are identified by size and color, as indicated by different spheres.

To better understand the defect production in GaAs, the numbers of antisite defects and atoms displaced into interstitial positions are shown in Fig. 5 as a function of time for the 10 keV cascade demonstrated above, where Ga and As components are plotted separately. The increase in the number of displaced atoms, N_d , during the collisional stage reaches a maximum at $t_{\text{peak}} \sim 0.5$ ps, after which N_d decreases in a recombination phase. As noted before, the number of displaced defects decreases only slightly to final values within 1.3 ps. However, the recombination of displaced atoms with vacancies is small within the relaxation phase, as shown in Figs. 4(a) and (b), and only 18% of the displaced atoms recombine with vacancies. Similar to other semiconductor compounds, most antisite defects are generated during the collisional phase, when the maximum in N_d is reached, and the increase in antisite defects is very small during relaxation. This may suggest that the formation of antisite defects is due to replacement collision sequences, although they are very short. However, the cascade lifetime, defined as the time during which the variation in the final number of defects can be neglected, is very short as ~ 1.2 ps, and the defects are quickly quenched, thus forming high disordered domains. Previously, several models have been proposed to explore the mechanisms associated with amorphization due to ion irradiation [34], including direct-impact amorphization within an individual collision cascade, the accumulation of defects due to cascade overlap, defect-stimulated nucleation, and growth processes, or a combination of these processes. The observed generation of amorphous pockets in GaAs, which are formed locally within a cascade, is likely to be associated with direct-impact amorphization in the model. Another important feature is that the number of Ga defects is roughly the same as that for As, which is expected because of the similar threshold energies for Ga and As in GaAs, i.e the threshold displacement energies are 13.75 eV for Ga and 14.3 eV for As averaged over more than 3600 simulated recoil events [25].

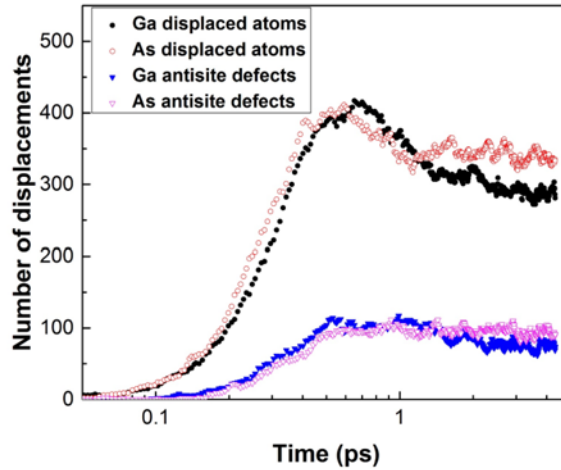


Fig. 5 The number of displaced atoms, including Ga and As displacements and antisites, as a function of time for the 10 keV cascade shown in Fig. 4.

Figure 6 shows the final defect distributions and cascade morphologies produced by 2, 5 and 20 keV cascades in GaAs. The defects generated by a PKA with an energy less than 2 keV distribute on one cascade region, and consist of interstitials and vacancies, rather than antisite defects, as demonstrated by Fig. 6(a). However, a PKA generates multiple sub-branches of the cascade along its path when its energy is larger than 2 keV, which is clearly displayed in Figs. 6(b) and (c), forming distinct regions separated from each other with a high energy density in the cores of the sub-branches. For example, a 5 keV PKA in Fig. 6(b) creates two distinct regions each of which has its own core of high defect density. This suggests that the nonlinear effects take place in high energy cascades in GaAs, which may be important in calculating the NIEL with effects not captured in the simplified Kinchin-Pease model.

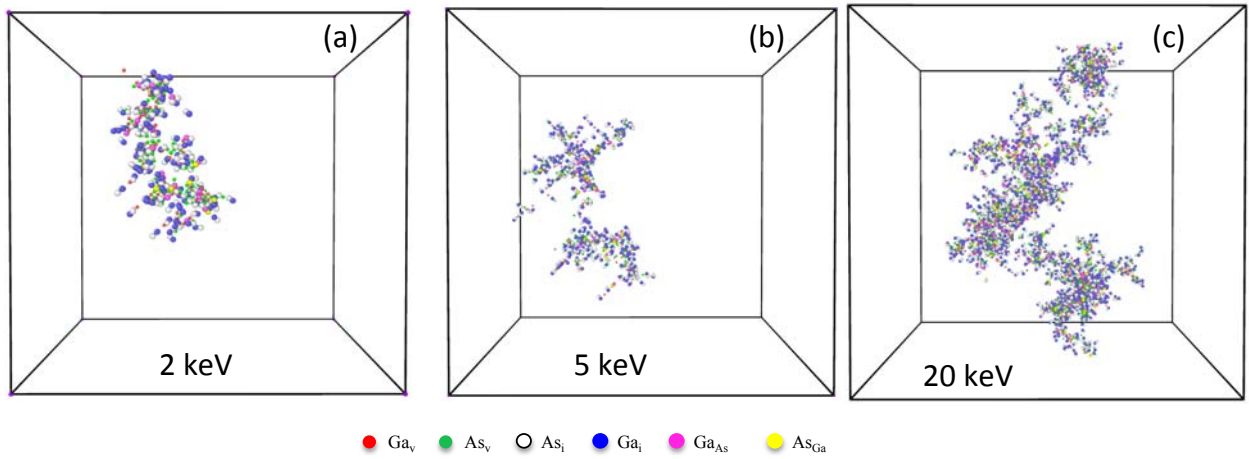


Fig. 6 The final defect states of (a) 2 keV, (b) 5 keV and (c) 20 keV cascade in GaAs from which can be clearly seen the transition from a single pocket of atomic displacements to multiple subcascades.

The final number of defects created in displacement cascades is an important outcome of MD simulations because of its applications to theories and models of radiation damage evolution. This parameter can be easily determined from MD simulations and compared with the standard formula of Norgett, Robison and Torrens [35] defined by

$$N_{NRT} = 0.8E_{PKA} / 2E_d \quad (8)$$

where E_{PKA} is the PKA energy that is elastically deposited into the target, and E_d is the mean threshold energy that is taken to be 14 eV [25]. Data for the final number of Frenkel pairs, N_F , at the end of the displacement cascades are shown as a function of PKA energy in Fig. 7, along with the NRT values for comparison. The number of Ga interstitials, As interstitials and antisite defects are presented separately, and the points denote the mean values for the displacement cascades investigated at the given energy. It is of interest to note that the total number of defects produced

in GaAs is generally much higher than that predicted by the NRT formula, in contrast to SiC where the total number of the defects is smaller than the NRT value [36]. This may be associated with the direct-impact amorphization that occurs in GaAs, which prevents the fast annihilation of interstitials with vacancies during the relaxation phase. The defect production efficiency, defined as the ratio of N_F to N_{NRT} , ranges from 3.0 to 5.0 and increases with increasing PKA energy, rather than decreasing with increasing PKA energy as revealed in SiC [36] and metals [34]. This suggests that defect production efficiency in GaAs is higher than that found in metals or alloys because of the absence of a thermal spike in GaAs. It is also clear that there exist two distinct regions of defect production, one exhibiting the linear behavior of cascades when PKA energy is less than 2 keV and a non-linear region with enhanced defect production related to the formation of amorphous domains for PKA energies larger than 2 keV, as shown in the insert of Fig. 7. This crossover in defect production may account for the different mechanisms for energy partition in GaAs. The NRT values are imposed for comparison. Data points are the mean values at each energy.

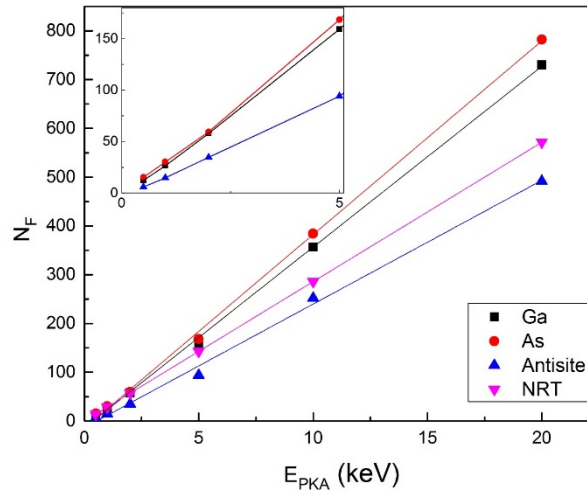


Fig. 7 The number of surviving defects produced in the cascades as a function of PKA energy, where Ga and As interstitials, as well as antisite defects, are presented separately.

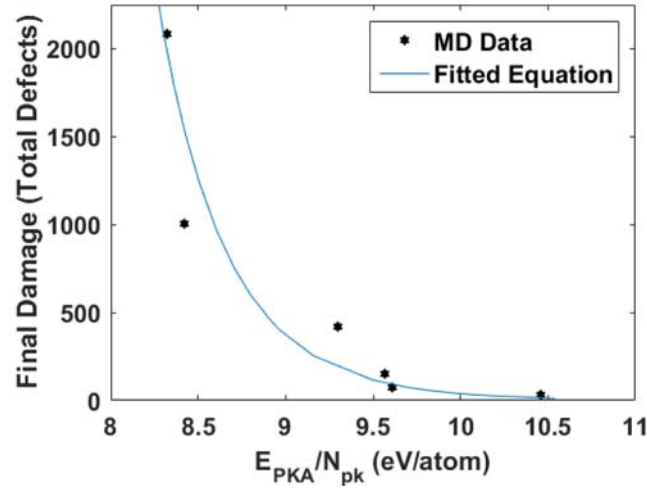


Fig. 8 The total defects of the final damages as a function of the energy density deposited by a PKA, where the solid line represents the fits to MD data.

4.2.2. Effective NIEL

Based on the MD simulations, the number of Frenkel pairs produced can be extrapolated into higher energies, and thus it is possible to develop a relationship describing defect production and PKA energy. Previous simulations of displacement cascades in a number of materials have revealed that the number of Frenkel pairs displays a power-law dependence on PKA energy, weakly depending on materials and temperature. If we assume that the energy transfer to atoms occurs just before the damage peak (maximum), the energy density deposited by a PKA is equal to $\rho_{ed} = E_{PKA} / N_{pk}$, where E_{PKA} is the PKA energy and N_{pk} is the number of displacements generated at the peak damage. The number of surviving defects (Frankel pairs produced) can be described by

$$N_F^{MD} = A (E_{PKA})^n \rho_{ed}^m \quad (9)$$

where the PKA energy, E_{PKA} , is given in keV. The dimensionless parameters A , n and m can be determined by fitting to the MD data, and the values for GaAs are approximately 7635.95, 2.1499 and 1.1108, respectively. The total number of defects, N_F^{MD} , that includes interstitials and antisites, is plotted as a function of energy density in Fig. 8, where the solid line indicates the values calculated by Eq. (9). It can be seen that our analytical model is relatively close to the MD simulations. N_F^{MD} decreases with increasing energy density, which is expected because a large number of atoms are displaced from their sites at higher PKA energies, giving rise to the lower energy density. Practically, a rate of degradation in electronic devices can be described by the number of defects in the materials, but experimentally, degradations are represented by the NIEL which is assumed to be proportional to the number of defects produced by irradiation. Combining Eqs. (5) and (9), the effective NIEL in GaAs is determined for incident proton, alpha and Xe

particles, and the results are shown in Fig. 9, along with other calculations for comparison. The striking fact is that the general behavior is very similar in all of these calculations, i.e. the NIEL increases with increasing incident energy until the peak NIEL and then decreases. Also, the peak position and magnitude of the NIEL strongly depend on the incident particles, and the peak NIEL shifts to higher energies with increasing mass of incident particles. For instance, the peak NIEL for Xe is more than 5000 times higher than that for protons, and the peak occurs at an energy that is about 1000 times higher than that for protons. Messenger et al. used a similar model to calculate the NIEL in numerous materials [26], including GaAs, but assumed that displacement damage is proportional to the kinetic energy of the recoil. Their results are also included in Fig. 9, as indicated by the dotted lines. Although the general tendency of the NIEL is similar, there appears to be distinguished differences at both low and high energies, which may point to fundamentally different mechanisms of displacement damage in GaAs. As described before, a PKA generates a single pocket of atomic displacements when its energy is below 2 keV, or single point defects when its energy is less than 500 eV, where the damage is in the linear regime of defect generation and is proportional to the recoil energy. This may provide an explanation for why the NIEL at low energies is in reasonable agreement with that calculated by Messenger et al [26]. For higher energies, the sub-branches or subcascades generated by recoil nuclei must be taken into account, which describes the non-linear behavior of defect production in GaAs and cannot be predicted by the simple Kinchin-Pease model. For instance, the number of atomic displacements by a 5 keV PKA in GaAs is, on average, around 421, that is about 3 times the number of displacements predicted by the Kinchin-Pease model. The multiple amorphous pockets formed within a cascade give rise to the number of defects produced, resulting in larger NIEL at high recoil energies than that determined by Messenger et al [26]. In addition, the NIEL determined using the simulation code based on transport of ions in matter transport of ions in matter (TRIM) code for incident protons from 0.2 to 2 MeV in GaAs [14] is added in Fig. 9 for comparison. The data points are very close to the NIEL of Messenger et al. and smaller than the calculations based on MD simulations, which is expected. In the TRIM calculation, the vacancy production rate as a function of position was combined with the total energy loss data to determine the vacancy production rate as a function of proton energy. It should be noted that TRIM calculations do not take defect kinetics (e.g. recombination) into account. The sub-cascade mechanisms outlined herein seem to overcompensate for any point defect kinetics ignored by TRIM. Since the vacancy concentration was converted to damage energy using the modified Kinchin-Pease approximation to yield the NIEL as a function of proton energy, it is not surprising that the NIELs calculated by Messenger et al. and TRIM are in good agreement. Nevertheless, we have developed an MD-based NIEL model to determine the NIEL in GaAs, which can be applied to a variety of incident particles. It is also suggested that further experimental measurements are needed for higher fidelity comparisons with this and other methods.

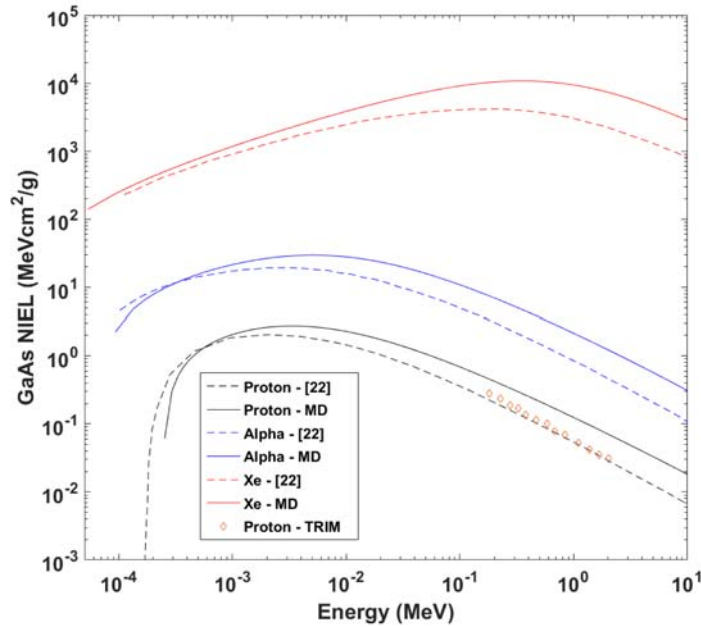


Fig. 9 The NIEL obtained based on the MD results for several different incident particles in GaAs, where the values of the NIEL calculated by an analytical approach [26] are imposed for comparison.

5. CONCLUSIONS

The threshold displacement energies for Ga and As atoms were investigated using a molecular dynamics method with a bond-order potential for GaAs, and the results demonstrated a weak dependence on the crystallographic direction in which the atom is displaced. The different types of lattice-atom vibrational modes and atomic sizes are believed to account for this slight dependence. By considering the crystallographic orientations of GaAs, a total of 3600 recoils are simulated to study the special distribution of threshold energies in four stereographic triangles. The threshold energy for As recoils ranged from 8 to 28 eV, while it ranged from 8 to 22 eV for Ga recoils. The average threshold along the directions whose crystallographic projections are located on the central part of a triangle is generally higher than on its sides. Nonetheless, it has also been shown that the average displacement energies were similar for both atoms, which is reasonable since the two atoms have similar physical properties like mass and short-range repulsion. Moreover, for low-energy displacements, the defect types generated by recoil events along low-index crystallographic directions are mostly in a simple form of Frenkel pairs. The separation distances of Frenkel pairs in these directions are mostly around 4.8 Å at an average of 4.69 Å except those along the [100] direction, which become shorter with a small threshold energy of 10 eV and a closer distance from the initial position to a stable octahedral site. However, complex defect configurations along some high-index directions are observed, which results in higher threshold energies.

Also, we have employed large-scale molecular dynamics (MD) simulations to study defect production and its detailed evolution for PKA energies from 500 eV to 20 keV in GaAs. At low energies, most surviving defects are single interstitials and vacancies, and only 20% of the interstitial population is contained in clusters. A PKA with an energy less than 2 keV generates a single pocket of atomic displacements, which is associated with the linear regime of displacement damage. Direct-impact amorphization occurs with a high degree of probability when PKA energies are larger than 2 keV, which involves non-linear defect production. The transition from linear to non-linear defect production plays an important role in the calculation of the NIEL in GaAs. Based on the MD results, we have further determined the damage density within a cascade core that is used to develop a model for calculating the NIEL in GaAs, which can then be used to predict the displacement damage degradation induced by space radiation on electronic components.

The calculated NIEL results are compared with the available data determined by different models. The agreement between our calculations and other values of the NIEL for protons is reasonably good at low energies, but there is a discrepancy at higher energies, which is expected because of non-linear effects neglected by the Kinchin-Pease model. The model developed in the present study provides a general method for accurately calculating the NIEL for fast neutrons, protons and other heavy particles, and can also be applied to other semiconductor materials.

REFERENCES

- [1] Joseph Callaway, Quantum Theory of the Solid State, Academic Press, Inc., New York, (1991).
- [2] R. Weatherford and W. T. Anderson, Jr., “*Historical perspective on radiation effects in III-V device*,” IEEE Trans. Nucl. Sci., **50**, 704 (2003).
- [3] J. S. Yoon, et al., “*GaAs photovoltaics and optoelectronics using releasable multilayer epitaxial assemblies*,” Nat., **465**, 329 (2010).
- [4] J. H. Warner, S. R. Messenger, R. J. Walters, G. P. Summers, J. R. Lorentzen, D. M. Wilt, and M. A. Smith, “*Correlation of electron radiation induced-damage in GaAs solar cells*,” IEEE Trans. Nucl. Sci., **53**, 1988 (2006).
- [5] W. Braunschweig, et al., “*Investigation of the radiation damage of GaAs detectors by neutrons and photons*,” Nucl. Instru. Methods Phys. Res. A, **372**, 111 (1996).
- [6] M. Samaras, P. M. Derlet, H. Van. Wygenhoven, and M. Victoria, “*Computer Simulation of Displacement Cascades in Nanocrystalline Ni*,” Phys. Rev. Lett., **88**, 125505 (2002).
- [7] M. A. Tschopp, K. N. Solanki, F. Gao, X. Sun, M. A. Khaleel, and M. Horstemeyer, “*Probing grain boundary sink strength at the nanoscale: Energetics and length scales of vacancy and interstitial absorption by grain boundaries in α -Fe*,” Phys. Rev. B, **85**, 064108 (2012).
- [8] D. Chen, F. Gao, and B. Liu, “*Grain boundary resistance to amorphization of nanocrystalline silicon carbide*,” Sci. Rep., **5**, 16602 (2015).
- [9] M. Lang, R. Devanathan, R. M. Toulemonde, and C. Trautmann, “*Advances in understanding of swift heavy-ion tracks in complex ceramics*,” Solid State and Mater. Sci., **19**, 39 (2015).
- [10] H. Y. Xiao, F. Gao, and W. J. Weber, “*Ab initio investigation of phase stability of $Y_2Ti_2O_7$ and $Y_2Zr_2O_7$ under high pressure*,” Phys. Rev. B, **80**, 212102 (2009).
- [11] F. Gao, H. Y. Xiao, X. T. Zu, M. Posselt, and W. J. Weber, “*Defect-enhanced charge transfer by ion-solid interactions in SiC using large-scale Ab Initio molecular dynamics simulations*,” Phys. Rev. Lett., **103**, 027405 (2009).
- [12] T. Diaz de la Rubia, and, G. H. Gilmer, “*Structural transformations and defect production in ion implanted silicon: A molecular dynamics simulation study*,” Phys. Rev. Lett., **74**, 2507 (1995).
- [13] E. A. Burke, et al., “*Energy dependence of proton-induced displacement damage in gallium arsenide*,” IEEE Trans. Nucl. Sci., **NS-34**, 1220 (1987).
- [14] G. P. Summers, E. A. Burke, P. Shapiro, S. R. Messenger, and R. J. Walters, “*Damage correlations in semiconductors exposed to gamma, electron and proton radiations*,” IEEE Trans. Nucl. Sci., **40**, 1372 (1993).
- [15] S. R. Messenger, M. A. Xapsos, E. A. Burke, R. J. Walters, and G. P. Summers, “*Proton displacement damage and ionizing dose for shielded devices in space*,” IEEE Trans. Nucl. Sci., **44**, 2169 (1997).

- [16] S. Lazanu, and I. Lazanu, “*Si, GaAs and diamond damage in pion fields with application to LHC,*” Nucl. Instrum. Meth. A, **419**, 570 (1998).
- [17] R. J. Walters, S. R. Messenger, H. L. Cotal, G. P. Summers, and E.A. Burke, “*Electron and proton irradiation-induced degradation of epitaxial InP solar cells,*” Solid State Electron., **39**, 797 (1996).
- [18] I. Jun, “*Effects of secondary particles on the total dose and the displacement damage in space proton environments,*” IEEE Trans. Nucl. Sci., **48**, 162 (2001).
- [19] S. R. Messenger, R. J. Walters, E. A. Burke, G. P. Summers, and M. A. Xapsos, “*NIEL and damage correlations for high-energy protons in gallium arsenide devices,*” IEEE Trans. Nucl. Sci., **48**, 2121 (2001).
- [20] F. Gao, D. J. Bacon, P. E. Flewitt, and T. A. Lewis, “*A molecular dynamics study of temperature effects on defect production by displacement cascades in α -iron,*” J. Nucl. Mater., **249**, 77 (1997).
- [21] K. Nordlund, J. Wallenius, and L. Malerba, “*Molecular dynamics simulations of threshold displacement energies in Fe,*” Nucl. Instr. Meth. Phys. Res. B, **246**, 322 (2006).
- [22] K. Uegami and K. Tamamura, “*Consequence of Orientation on the Single Crystal Diamond Cutting Tool,*” Progress in Precision Engineering” (Ed. by P. Seyfried, et al., Springer Berlin Heidelberg, 1991).
- [23] K. Albe, K. Nordlund, J. Nord, and A. Kuronen, “*Modeling of compound semiconductors: Analytical bond-order potential for Ga, As, and GaAs,*” Phys. Rev. B, **66**, 035205 (2002).
- [24] J. P. Biersack, and J. F. Ziegler, “*Refined universal potentials in atomic collisions,*” Nucl. Instr. & Meth., **194**, 93 (1982).
- [25] F. Gao, N. Y. Chen, E. Hernandez-Rivera, D. H. Huang, and P. D. LeVan, “*Displacement damage as revealed by computer simulations and effective non-ionizing energy loss in GaAs,*” J. Appl. Phys., 121, 09514, 2017.
- [26] R. S. Messenger, et al., “*NIEL for heavy ions: An analytical approach,*” IEEE Trans. Nucl. Sci., **50**, 1919 (2003).
- [27] R. S. Messenger, et al., “*NIEL and damage correlations for high-energy protons in gallium arsenide devices,*” IEEE Trans. Nucl. Sci., **48**, 2121 (2001).
- [28] J. Lindhard, M. Scharff, and H. E. Schiott, “*Range concepts and heavy ion ranges,*” Mat. Fys. Medd. Dan. Vid. Selsk., **33**, 1 (1963).
- [29] M. Nastasi, J. M. Mayer, and J. K. Hirvonen, “*Ion-Solid Interactions: Fundamentals and Applications,*” New York, Cambridge University Press (1996).
- [30] E. Holmström, A. Kuronen, and K. Nordlund, “*Threshold defect production in silicon determined by density functional theory molecular dynamics simulations,*” Phys. Rev. B, **78**, 045202 (2008).
- [31] A. L. Barry, R. Maxseiner, R. Wojcik, M. A. Briere, and D. Braunig, “*An improved displacement damage monitor LED,*” IEEE Trans. Nucl. Sci., **37**, 1726 (1990).
- [32] K. Nordlund, J. Peltola, J. Nord, and J. K. R. S. Averbach, “*Defect clustering during ion*

- irradiation of GaAs: Insight from molecular dynamics simulations*,” J. Appl. Phys., **90**, 1710 (2001).
- [33] F. Gao, and W. J. Weber, “*Atomic-scale simulation of 50 keV Si displacement cascades in β -SiC*,” Phys. Rev. B, **63**, 054101 (2000).
- [34] W. J. Weber, “*Models and mechanisms of irradiation-induced amorphization in ceramics*,” Nucl. Instrum. Methods Phys. Res. B, **166–167**, 98 (2000).
- [35] M. J. Norgett, M. T. Robinson, and I. M. Torrens, “*A proposed method of calculating displacement dose rates*,” Nucl. Eng. Des., **33**, 50 (1975).
- [36] F. Gao, W. J. Weber, and R. Devanathan, “*Atomic-scale simulation of displacement cascades and amorphization in β -SiC*,” Nucl. Instrum. Meth. Phys. Res. B, **180**, 176 (2001).

LIST OF ACRONYMS

As	Arsenide
BOPs	Bond-order potentials
eV	Electron volt
GaAs	Gallium arsenide
InP	Indium phosphide
keV	1000 eV
MD	Molecular dynamics
MOLDY	MOLEcular Dynamics simulation code
NF	the final number of Frenkel pairs
NIEL	Non-ionizing energy loss
PKA	Primary knock-on atom
Ps	Pico-second
Rf	Fitting parameter
SIA	Self-interstitial atoms
SiC	Silicon carbide
Si	Silicon
SREC	Space radiation effects community
TRIM	Transport of ions in matter
ZBL	Ziegler-Biersack-Littmark

DISTRIBUTION LIST

DTIC/OCF	
8725 John J. Kingman Rd, Suite 0944	
Ft Belvoir, VA 22060-6218	1 cy
AFRL/RVIL	
Kirtland AFB, NM 87117-5776	2 cys
Official Record Copy	
AFRL/RVSW/David Cardimona	1 cy